MIT Open Access Articles

Variability and anatomical specificity of the orbitofrontothalamic fibers of passage in the ventral capsule/ventral striatum (VC/VS): precision care for patient-specific tractography-guided targeting of deep brain stimulation (DBS) in obsessive compulsive disorder (OCD)

CrossMark

Variability and anatomical specificity of the orbitofrontothalamic fibers of passage in the ventral capsule/ventral striatum (VC/VS): precision care for patient-specific tractography-guided targeting of deep brain stimulation (DBS) in obsessive compulsive disorder (OCD)

Nikolaos Makris [1,2,3,4] · Yogesh Rathi [1,2] · Palig Mouradian [1] · Giorgio Bonmassar [1] ·
George Papadimitriou [1] · Wingkwai I. Ing [1] · Edward H. Yeterian [5] · Marek Kubicki [1,2] ·
Emad N. Eskandar [1] · Lawrence L. Wald [1] · Qiuyun Fan [1] · Aapo Nummenmaa [1] ·
Alik S. Widge [1,6] · Darin D. Dougherty [1]

Abstract Deep Brain Stimulation (DBS) is a neurosurgical procedure that can reduce symptoms in medically intractable obsessive-compulsive disorder (OCD). Conceptually, DBS of the ventral capsule/ventral striatum (VC/VS) region targets reciprocal excitatory connections between the orbitofrontal cortex (OFC) and thalamus, decreasing abnormal reverberant activity within the OFC-caudate-pallidal-thalamic circuit. In this study, we investigated these connections using diffusion magnetic resonance imaging (dMRI) on human connectome datasets of twenty-nine healthy young-adult volunteers with two-tensor unscented Kalman filter based tractography. We studied the morphology of the lateral and medial orbitofrontothalamic connections and estimated their topographic variability within the VC/VS region. Our results showed that the morphology of the individual orbitofrontothalamic fibers of passage in the VC/VS region is complex and inter-individual variability in their topography is high. We applied this method to an example OCD patient case who underwent DBS surgery, formulating an initial proof of concept for a tractography-guided patient-specific approach in DBS for medically intractable OCD. This may improve on current surgical practice, which involves implanting all patients at identical stereotactic coordinates within the VC/VS region.

✉ Nikolaos Makris
nikos@cma.mgh.harvard.edu

[1] Departments of Psychiatry, Neurology, Neurosurgery and Radiology, Center for Morphometric Analysis, Athinoula A. Martinos Center for Biomedical Imaging, Massachusetts General Hospital, Building 149, 13th Street, Charlestown, MA 02129, USA

[2] Department of Psychiatry, Psychiatry Neuroimaging Laboratory, Brigham and Women's Hospital, Harvard Medical School, Boston, MA, USA

[3] McLean Imaging Center, McLean Hospital, Harvard Medical School, Boston, MA, USA

[4] Department of Anatomy and Neurobiology, Boston University School of Medicine, Boston, MA, USA

[5] Department of Psychology, Colby College, Waterville, ME, USA

[6] Picower Institute for Learning & Memory, Massachusetts Institute of Technology, Cambridge, MA, USA

Introduction

Obsessive-compulsive disorder (OCD) is a chronic mental illness affecting 4–7 million people in the U.S. Patients are impaired in multiple Research Domain constructs (Cuthbert and Insel 2010, 2013) including Habit (perseverative compulsive behaviors), Sustained Threat (anxiety in response to obsessional thoughts that they know are untrue), and Reward Learning (inability to learn to resist obsessions/compulsions despite negative consequences). Medication and behavioral therapies yield inadequate symptom relief in 50–70 %

🖄 Springer

(Greist et al. 1995; Koran et al. 2007; Pallanti et al. 2002; Pittenger and Bloch 2014) of patients. As a result, OCD remains a leading worldwide cause of disability, equivalent in impact to more visible disorders such as schizophrenia (Ayuso-Mateos 2002). Roughly one-third of patients are unable to work due to their symptoms (Mancebo et al. 2008) and their caregivers report profound, life-impairing stress (Laidlaw et al. 1999). The clinical syndrome and the underlying constructs have been linked to a set of cortico-striato-thalamo-cortical (CSTC) loops, circuits that subserve goal-directed action, learning, and motivation (Ahmari et al. 2013; Anticevic et al. 2014; Burguiere et al. 2013; Dougherty et al. 2010; Pauls et al. 2014; Posner et al. 2014). It is not known which loops are most important in OCD, but the orbitofrontal cortex (OFC) in particular is repeatedly implicated by neuroimaging studies as a hub, as are ventromedial prefrontal (vmPFC) and anterior cingulate (ACC) cortex (Dougherty et al. 2010; Milad and Rauch 2012).

In cases of medically intractable OCD, neurosurgical treatment is an option for reducing symptom burden and increasing quality of life. Although, given its limited application to date it is still too early to know with clarity how beneficial this procedure is, our clinical experience and of others (Greenberg et al. 2010a) have shown that approximately one-third of the patients had meaningful clinical improvement, another third showed partial clinical response while the remainder did not show any meaningful response. Deep brain stimulation (DBS) of the ventral capsule/ventral striatum (VC/VS) region may target reciprocal excitatory connections between OFC and thalamus, decreasing reverberant feedback activity within the OFC-caudate-pallidal-thalamic circuit, leading to therapeutic gains (Greenberg et al. 2010b). More specifically, it is thought that the OFC connections with the thalamus are the most relevant in OCD pathophysiology (Fineberg et al. 2010; Graybiel and Rauch 2000). The VC/VS target is not a single identifiable anatomical structure, but includes both white matter of the caudoventral part of the anterior limb of the internal capsule (ALIC) and the shell of the nucleus accumbens. Fibers of passage in this region connect dorsal prefrontal cortex (DPFC), dorsal anterior cingulate cortex (dACC), orbitofrontal cortex (OFC) and ventromedial prefrontal cortex (vmPFC) with the thalamus (principally mediodorsal, anterior medial, medial pulvinar, and midline-intralaminar nuclei), amygdala, hypothalamus and brainstem (substantia nigra, ventral tegmental area, raphe nuclei and peduncolopontine tegmental nucleus). The trajectories of these fibers of passage show a characteristic general pattern of topographic organization in VC/VS, but the individual projections and bundles overlap considerably (Jbabdi et al. 2013; Lehman et al. 2011; Yang et al. 2015). In DBS practice, anatomical inhomogeneity in VC/VS results in the stimulation of multiple different structures by implanted electrodes. Unless visualization of the various fiber tracts in this region is done in a manner that

reveals pathway specificity, there will be little clarity regarding target engagement or the correlation of any specific circuitry to therapeutic effect. We identified this problem and addressed it to a certain extent in two recent papers examining which gray and white matter structures were lesioned by subcaudate tractotomy in a cohort identified from a Massachusetts General Hospital database of patients maintained since 1992 (Yang et al. 2014) and mapping the anatomy of fibers of passage in the VC/VS region in normal subjects using DTI probabilistic tractography (Yang et al. 2015). Probabilistic tractography is useful for a general understanding of the topographic arrangement of the fibers of passage.

Current surgical practice involves implanting all patients at identical stereotactic coordinates within the VC/VS region. Thus, DBS for OCD as currently practiced lacks specificity with respect to targeted engagement of individual fiber tracts. From a purely anatomical perspective, another important factor that adds complexity to the specificity of fiber tract target engagement is the morphology of individual fiber tracts. Along their trajectories, as fiber tracts course from origin toward their termination, they deploy their fibers in the form of a "cloud." Although these clouds of fibers run side-by-side, they partially intertwine and share the same space, making it highly difficult to discern a specific fiber tract with clarity. Another highly relevant problem in DBS target engagement is inter-subject variability, which increases the probability of misplacement of the implant within the VC/VS region. For DBS to enable optimal target engagement and therapeutic efficacy, this surgical procedure should become patient-specific. Varying the specific implant coordinates based on tractography in individual patients would be one way to achieve that specificity.

In this study, given the relevance of the orbitofrontothalamic circuitry in OCD pathophysiology, we adressed issues of the anatomical connectivity between the OFC and the thalamus. We mapped the lateral orbitofrontothalamic (lOFC-thal) and the medial orbitofrontothalamic (mOFC-thal) connections and elucidated the topographic relationships of these two fiber connections within the VC/VS region in humans. We measured the inter-individual anatomical variabillity of lOFC-thal and mOFC-thal connections in a sample of twenty-nine individuals using two-tensor diffusion tractography of Connectome data and data from an OCD DBS patient. Our results represent an initial proof of concept indicating the relevance of a tractography-guided patient-specific approach in DBS neurosurgery for OCD.

Methods

We used magnetic DTI-based tractography in 29 human subjects to study the fibers of passage at the VC/VS area in the

caudoventral region of the anterior limb of internal capsule (ALIC), which are considered to be critical for DBS in OCD. To this end we accomplished three goals: a) we delineated the lateral and medial orbitofrontal connections with the thalamus in 29 healthy human volunteers and generated a database of biophysical parameters, such as fractional anisotropy (FA), axial diffusivity (AD), radial diffusivity (RD) and volume for the lateral and medial orbitofrontothalamic tract; b) we mapped the variabilty of the lateral and medial orbitofrontothalamic tract in 29 human datasets and generated a means of measuring and visualizing the variablity of these fibers of passage; c) finally, we illustrated the relevance of these observations in a case study of a patient with OCD who had undergone DBS in the VC/VS region.

Subjects

Healthy subjects Twenty-nine healthy subjects, 15 males, 20 to 59 years of age (age 32 on average) and 14 females, 20 to 44 years of age (age 29.5 on average) participated in the study. None of the subjects presented with a diagnosed neurological disorder or history of alcohol or other drug dependency. This study was approved by the Institutional Review Board (IRB) at Massachusetts General Hospital (MGH).

Patient The patient was a female approximately 30 years of age at the time of DBS implant. She reported symptoms of OCD with onset in her teenage years. At the time of presentation, these had not responded to medication, including trials of clomipramine and multiple serotonergic agents. Her symptoms had not reliably responded to exposure and response prevention therapy. She was unable to work or engage in substantial activities outside the home due to her symptoms. Following bilateral VC/VS DBS implant and approximately 6 months of DBS setting titration, she reported a 35 % decrease in her Yale-Brown Obsessive-Compulsive Score (YBOCS). She was able to return to formal educational and occupational activities. She experienced a brief period of hypomania during initial DBS titration, which did not recur once dose was adjusted appropriately. This study was approved by the MGH IRB.

MRI procedures

MRI for healthy subjects All subjects were scanned on a Siemens 3 Tesla Connectom at the MGH A. Martinos Center for Biomedical Imaging. We acquired multi-shell data with a spin-echo echo planar imaging (EPI) pulse sequence (TR = 8800 ms, TE = 57 ms, 96 slices, 21^2 cm^2 field of view, 1.5 mm isotropic voxels, at multiple b values of 1000, 3000, 5000 and 10,000 s/mm^2). Fiber tracts were sampled in 3D-Slicer (v2.7, www.slicer.org), using a multi-tensor tractography algorithm (Malcolm et al. 2010) as dicussed in

more detail below. We acquired diffusion scans to examine white matter integrity and perform tractography: two 128-direction (for a total of 256 directions) diffusion imaging sequences (TR = 8800 ms, TE = 57.0 ms, 96 slices, GRAPPA 3, with 1.5 mm isotropic voxels, at b-value 5000 s/mm^2 (Setsompop et al. 2013). Most diffusion scans include fewer directions (60 vs. 256), low spatial resolution (about 2 mm isotropic voxel size), and have dramatically lower b-values (700 or lower vs. 5000 s/mm^2), which requires the use of limited diffusion tensor imaging (DTI) models. The fine resolution, high number of directions, and high b value afforded by the state-of-the-art sequences possible with the Connectome scanner allow us to (1) fit advanced diffusion imaging models (Rathi et al. 2013) that can more precisely resolve the particular direction of a fiber bundle, and (2) perform tractography analyses, which can follow bundles all the way to their terminus region in gray matter through voxels where fibers bend or cross.

We used the data publicly available from the MGH human connectome project (MGH-HCP), where very high gradient strengths were used to obtain high b-values with reasonable SNR. These additional data can be useful to obtain a better estimate of the fiber crossings and hence were used in our work. Further, utilizing all of the data available can provide a better fit and provide a better estimate of the fiber orientation rather than using only part of the acquired data (e.g., using only the 2000 or 3000 b-value data).

Postmortem human head We utilized these datasets for illustration purposes by enhancing the anatomy of the thalamus and the VC/VS region by means of the high resolution we were able to achieve. The ex-vivo datasets were collected as 7 Tesla (7 T) T2* and Connectome dMRI data (Bonmassar and Makris 2015). Specifically, using a high-resolution T1-weighted dataset of an ex-vivo human brain, fixed in periodate-lysine paraformaldehyde (PLP), using a 7 Tesla Siemens scanner with a 3D FLASH (0.4^3 mm^3 resolution, 512^2 matrix, FoV 205 mm, 352 slices, FA 30°, TR = 35 ms, TE = 10.2 ms, 32 channel head array, Tacq = 1 h 45 min), we were able to parcellate the thalamus into several regions of interest (ROIs) (Andrew and Watkins 1969; Talairach et al. 1957). Taking advantage of the high resolution of this dataset, cortical and subcortical, viz. caudate nucleus, putamen, internal/external globus pallidus, nucleus accumbens septi and thalamus, parcellation was done using visible anatomical landmarks as per Makris and colleagues (Makris et al. 1999) and with the aid of atlases of the human thalamus and midline telencephalic and diencephalic nuclei (Andrew and Watkins 1969; Talairach et al. 1957). This was relevant in providing a more fine-grained understanding of the origins and terminations of the different orbitofrontal fiber tracts with specific nuclear groups of the thalamus. We also acquired diffusion

imaging data using the Siemens 3 Tesla "Skyra Connectom" at the MGH A. Martinos Center for Biomedical Imaging with a spin echo EPI sequence (1.5^3 mm^3 resolution, 140^2 matrix, FoV 210 mm, 95 slices, 128 diffusion directions at 5000 s/mm^2 and 10 b = 0 acquisitions, TR = 8800 ms, TE = 57 ms, 3x GRAPPA acceleration, 64 channel head array, with acquisition time approximately 22 min) to perform tractography of the orbitofrontothalamic connections.

Patient neuroimaging Preoperative MRI and postimplantation computed tomography (CT) scans were acquired in a patient under Institutional Exemption Device (IDE) as follows. *Preoperative MRI* Structural T1-weighted MEMPRAGE scan was acquired on Siemens TrioTim (TR: 2.53 s; Multi-Echo TE: 1.64/3.5/5.36/7.22 ms; TI: 1.2 s; Flip Angle: 7; FoV: 256 mm; 176 sagittal slices; Voxel Size: 1^3 mm^3). Diffusion scan was acquired on Siemens TrioTim (TR: 9.04 s; TE: 87 ms; Flip Angle: 90°; FoV: 213 mm; 72 axial slices; b-value 700 s/mm^2, Voxel size: 1.9 ^{3} mm^3). *Postimplantation CT* After electrode implantation, we collected high-resolution, non-contrast, thin slice CT with 1 mm thickness contiguous axial slices for full-head coverage. Subsequently, the CT scan was *co-registered* with the preoperative MRI to allow superimposition of the implanted electrodes on the MRI space. This allows visualization of the implants in relationship to the subject's brain anatomy. We used FNIRT, FSL's non-linear co-registration tool.

We demonstrated the variability of the VC/VS fibers in healthy subjects using the best dataset available. These data have very high spatial resolution and may allow more accurate measurements, making the estimation of the tracts more robust and reliable. Such advanced protocols are not currently available for scanning DBS patients. Further, the patient data were acquired before the MGH connectome was built. While the study on variability of the VC/VS tracts is quite reliable, the sub-optimal data used for the patient can affect construction of the VC/VS fibers of passage.

Parcellation of cortical and subcortical regions of interest (ROIs)

To define the cortical ROIs in the brain in general and in the orbitofrontal cortical (OFC) region in particular, namely the lateral OFC (lOFC) and medial OFC (mOFC), we carried out analyses using algorithms in the publicly available FreeSurfer software package (http://www.martinos.org/freesurfer) (Dale et al. 1999; Fischl and Dale 2000; Fischl et al. 1999). The T1-weighted images from each subject were motion-corrected, averaged, and normalized for intensity; subsequently, automated computational reconstruction of brain surface and segmentation of the cortical and subcortical structures was done. Finally, segmentation and automatic labeling of cortical (i.e., cortical parcellation) and subcortical regions

(Desikan et al. 2006; Fischl et al. 2002, 2004) were done by implementing algorithms as described by Fischl and colleagues (Dale et al. 1999; Fischl and Dale 2000; Fischl et al. 1999).

Tractographic delineation of lateral and medial orbitofrontothalamic (lOFC-thal and mOFC-thal) fiber tracts

Fiber tractography was performed using a multi-tensor tractography algorithm (Malcolm et al. 2010). This algorithm uses tractography to drive the local fiber model estimation, i.e., model estimation (in this case, the multiple tensors) is done while tracing a "fiber" from seed to termination. It must be pointed out that "fiber" is a computational term used throughout this study to denote "virtual fibers". Because existing techniques independently estimate the model parameters at each voxel (throughout the brain) prior to tractography, there is no running knowledge of confidence in the estimated model fit. Furthermore, noise can significantly affect the estimated model parameters particularly in the case of multi-tensor models, which others including Malcolm and colleagues (Malcolm et al. 2010) and Baumgartner and colleagues (Baumgartner et al. 2012) have compared with existing methods. Malcolm et al. (Malcolm et al. 2010) describe an algorithm that formulates fiber tracking as a recursive estimation process, wherein the estimate at each step of tracing the fiber is guided by previous estimates. In this model, tractography is performed within a filter framework that uses a discrete mixture of Gaussian tensors to model the signal. Starting from a seed point, each fiber is traced to its termination using an unscented Kalman filter to simultaneously fit the local model to the signal and propagate it in the most consistent direction. Despite the presence of noise and uncertainty, this method provides a causal estimate of the local structure at each point along the fiber. Furthermore, because each iteration begins with a near-optimal solution based on the previous estimation, the convergence of model fitting is improved and local minima are naturally avoided. Another important aspect of this algorithm is that it provides a measure of confidence (a covariance matrix) in the estimation of the parameters at each step, which can remove false positives in tractography. This approach reduces signal reconstruction error and significantly improves the angular resolution at crossings and branchings. Because it enables detection of two eigenvalues in a voxel, this method resolves the problem of crossing fibers, allowing fiber tracing in areas known to contain such crossing and branching (Rathi et al. 2010). Subsequently, the white matter query language (WMQL) was used (Wassermann et al. 2013) to obtain two different fiber tracts for each hemisphere by

selecting only the fibers that passed through specific regions for each lateral and medial orbitofrontal-thalamic connection. The two fiber tracts included the following regions: the cortex of the lateral orbitofrontal cortex, medial orbitofrontal cortex and thalamus (Figs. 1 and 2). Tracts were obtained by seeding once per voxel. To ensure the anatomical accuracy of lOFC-thal and mOFC-thal reconstructions, all cases were inspected. Differentiating the thalamic connections of the lOFC-thal and mOFC-thal from those of other regions such as the anterior cingulate (ACC) and ventromedial prefrontal (vmPFC) cortex is feasible using tractography as shown in Fig. 3.

It should be noted that it is generally accepted that not more than 3 fiber crossings can be reliably detected at a given voxel location. Further, as reported by Behrens et al., (2007), a majority of the white matter tends to have 2 crossing fibers, with some regions known to have 3 crossings (in the centrum semiovale). In the areas we analyze in this work (lOFC and mOFC), we expect at most two-fiber crossing, hence we used the two-tensor model. While this is definitely a limitation of our method, it is well-known that fitting a multi-exponential model to the data is fraught with several local minima resulting in several solutions. In the proposed method, we

provide a robust way to estimate the two tensors using a running knowledge of the previous estimate as well as using the covariance of the estimated parameters to determine the best possible solution. Thus, despite the limitations of our method overall, we believe it can provide a good estimate of the fiber tracts of the orbitofrontal fibers.

Assessment of inter-subject variability of fibers of passage in the VC/VS region

We assessed the variability of the lateral orbitofrontothalamic and medial orbitofrontothalamic fibers of passage at the VC/VS region using two complementary approaches. One way of demonstrating variabilty was a histogram that represents the distribution of tracts as a function of distance (in mm) from their overall center at the coronal level of the anterior commissure (ac). Another was through a heat map, representing the probability distribution of the fiber tracts at the same coronal level. In addition, we computed the mOFC and lOFC in each individual's subject space using Freesurfer, and subsequently mapped the individual center-of-mass trajectories to a common MNI space to compute variability across the population.
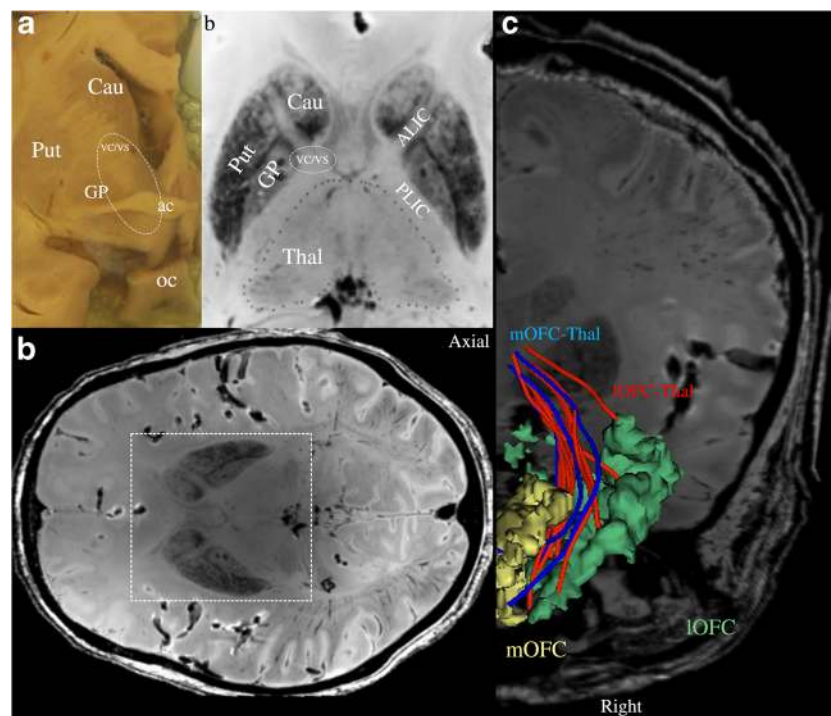

Fig. 1 Anatomy of the ventral capsule/ventral striatum (VC/VS) region targeted for DBS in OCD. Panels a and b show the topographic relationships of the caudate nucleus (Cau), putamen (Put) and globus pallidus (GP). Panel a is a gross coronal section at the level of the anterior commissure (ac), whereas b is an axial section of a high-resolution T2-MRI dataset of a postmortem human head. Panel c shows the fibers of passage connecting the thalamus with the lateral orbitofrontal (lOFC, in *red*) and medial orbitofrontal (mOFC, in *blue*) cortex at the ac coronal level in a high-resolution T2-MRI dataset of a postmortem human head. These fibers were extracted using diffusion tractography (see text). The parcellation of the orbitofrontal cortex into lateral and medial regions of interest (ROIs) was done following FreeSurfer conventions as by Desikan and colleagues (2006). In the Desikan et al. anatomical convention, lOFC ROI corresponds to the central OFC (cOFC) and lateral OFC (lOFC) ROIs of the Lehman et al. (2011) convention, whereas the mOFC ROI corresponds roughly to the ventromedial prefrontal cortex (vmPFC) and medial OFC (mOFC) ROIs of Lehman and colleagues. oc= optic chiasm

Fig. 2 Panel **a** shows the two orbitofrontothalamic connections in 3-D using as background a coronal section of a T1-weighted MRI dataset at the anterior commissure (ac) level. Panels **b** and **c** show 3-D reconstructions of the two fiber tracts connecting the thalamus with the lateral orbitofrontal (lOFC, in *red*) and medial orbitofrontal (mOFC, in *blue*) cortex. R = right; L = left
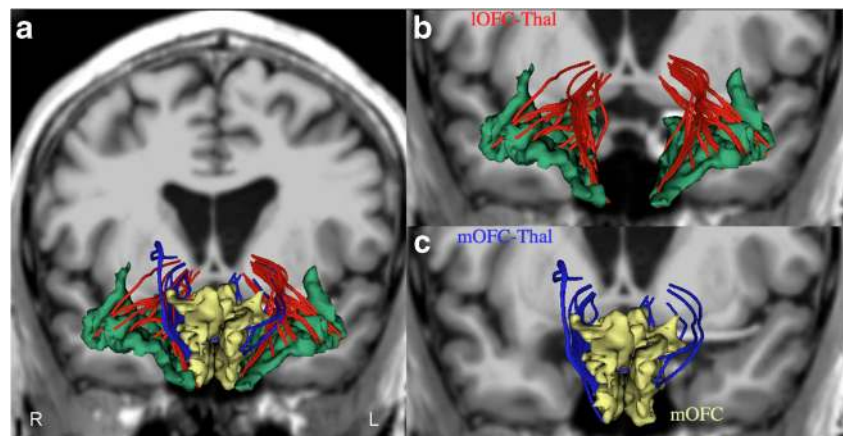
Quantitative analyses

Measurements of volume, length, mean FA, mean AD and mean RD of the left and the right lOFC-thal and mOFC-thal connections were obtained in 29 healthy human subjects. The dMRI biophysical parameters of FA, AD and RD may relate to fiber tract coherence and integrity (Basser 2004; Song et al. 2002, 2003). *Symmetry index (SI)* (SI = [Left- Right] / 0.5 (Left + Right]; (Galaburda et al. 1987) for left and right middle longitudinal fascicle (MdLF) for measures of volume, mean FA, mean AD and mean RD were calculated for each individual, and across subjects.

Fig. 3 VC/VS is not a single identifiable anatomical structure but a region containing fibers of passage that include principally prefrontal connections of the dorsal prefrontal cortex (DPFC), dorsal anterior cingulate cortex (dACC), orbitofrontal cortex (OFC) and ventromedial prefrontal cortex (vmPFC) with the thalamus (mediodorsal, midline-intralaminar and anterior medial nuclei), amygdala, hypothalamus and brainstem (substantia nigra, ventral tegmental area, raphe nuclei and peduncolopontine tegmental nucleus). With respect to obsessive-compulsive disorder, the connections of lateral orbitofrontal cortex with the thalamus are considered to play a critical role in its pathophysiology
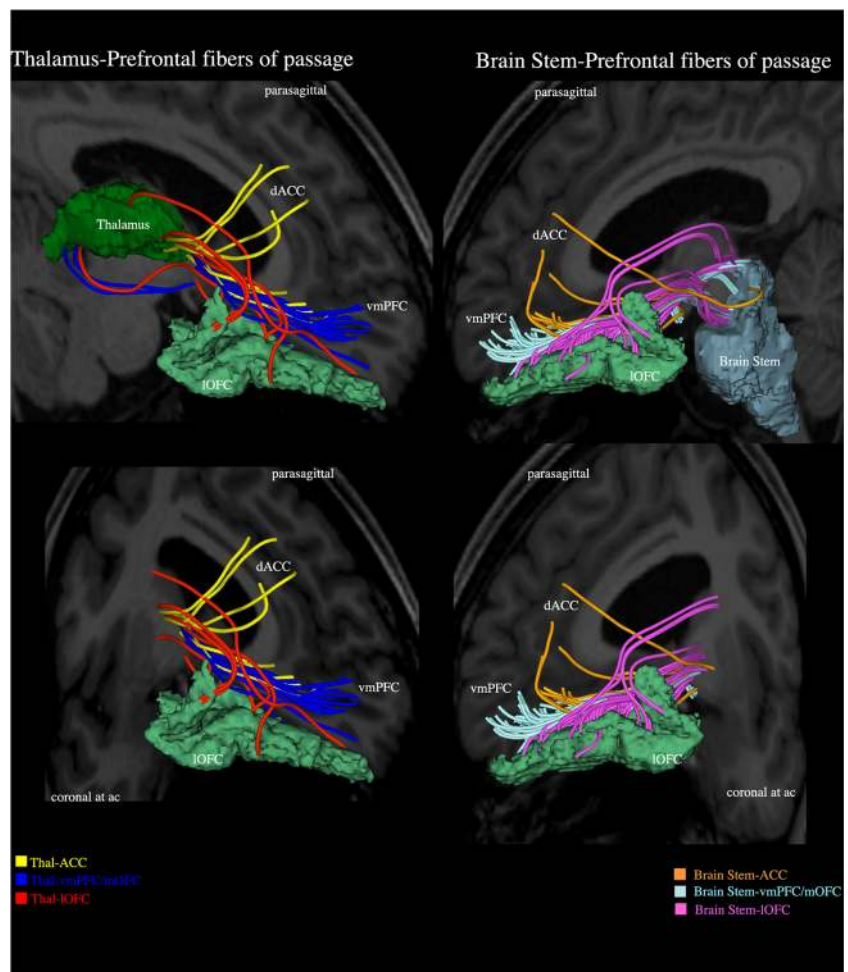
Results

Delineation and generation of a database of biophysical parameters and volume of the lateral and medial orbitofrontothalamic connections We were able to delineate the fibers of passage in VC/VS. In Fig. 1 we illustrate the anatomy of the VC/VS region using gross dissectional information as well as gray matter and fiber tract anatomical reconstruction from high-resolution datasets of a postmortem human head. The VC/VS at the caudoventral part of the ALIC is in proximity to the ventral caudate nucleus, the medial putamen and globus pallidus, and the shell of the nucleus accumbens. We also measured the volume, length and other biophysical parameters of the lOFC-thal and mOFC-thal connections, such as FA, AD and RD, as reported in Table 1. We were also able to distinguish connections between the lateral and medial OFC with the mediodorsal, midline-intralaminar and pulvinar nuclei of the thalamus. In Fig. 2 we show the result of tractographic analysis in one of the 29 healthy subjects who participated in this study. Although there is a multiplicity of fiber tracts in the VC/VS region connecting the frontal cortex with subcortical structures (Fig. 3), the fibers of passage of highest priority in OCD are thought to be those that convey the connections of the OFC, in particular its lateral portion (i.e., lOFC) (Fineberg et al. 2010; Graybiel and Rauch 2000; Greenberg et al. 2010b). With respect to the lOFC-thal and mOFC-thal connections, the parcellation of the thalamus into several regions allowed a fine-grained identification of the origin and termination of these fibers (Table 2).

Assessment of inter-subject variability of fibers of passage in the VC/VS region

The results of inter-subject variability of the lateral orbitofrontothalamic fibers of passage at the VC/VS region are shown in Figs. 4, 5 and 6 (tractography in 3-D and 2-D single slice at ac coronal representations in Fig. 4; specifically as histograms of the COMs as a function of distance from the overall COM in Fig. 5; as heat maps in Fig. 6). It should be noted that as shown in the heat maps, the vast majority of fibers of passage are above the anterior commissure-posterior commissure (ac-pc) plane, with very few below this plane.

DBS electrode placement and targeting in the VC/VS region in patients with OCD

We undertook this study to understand the variation in human VC/VS, with an eye towards developing better targeting algorithms for DBS placement in OCD. We therefore performed the same reconstruction on scans from a patient with OCD who underwent DBS with bilateral electrode placement in

Table 1 Quantitative measures of volume, length and biophysical parameters, specifically fractional anisotropy (FA), axial diffusivity (AD) and radial diffusivity (RD) of the two fiber tracts connecting the thalamus with the lateral orbitofrontal (lOFC) and medial orbitofrontal (mOFC) cortex

	Volume			FA			AD			RD			Length (mm)		
	Left	Right	SI	Left	Right	SI	Left	Right	SI	Left	Right	SI	Left	Right	SI
lOFC-thal															
Mean	1635.86	1506.19	0.08254	609.879	624.587	-0.024	1974.2	2027.96	-0.027	617.919	603.422	0.02374	73.1399	70.5921	0.03545
STD	1053.77	990.005	0.0624	38.0843	29.3822	0.25797	143.338	142.585	0.00527	88.2911	40.9007	0.73364	7.79813	7.26969	0.07014
mOFC-thal															
Mean	767.931	968.414	-0.231	597.173	623.425	-0.043	1982.56	2069.04	-0.043	637.035	617.604	0.03097	78.656	74.6966	0.05164
STD	500.056	706.153	-0.342	46.8497	42.4902	0.09759	135.172	144.165	-0.064	71.1418	48.8443	0.37167	12.1265	9.79099	0.21312

The symmetry index (SI) was estimated as follows: SI = (Left - Right) / 0.5 (Left + Right); STD = standard deviation

Table 2 Thalamic connectivity of the orbitofrontal cortex

Thalamic Nuclei	References
Anterior Nuclear Group Anterior Medial Nucleus	Arikuni et al. (1983)
	Barbas et al. (1991)
	Goldman-Rakic and Porrino (1985)
	Hsu and Price (2007)
	Morecraft et al. (1992)
	Xiao and Barbas (2002)
	Xiao et al. (2009)
Medial Nuclear Group Dorsomedial Nucleus	Arikuni et al. (1983)
	Barbas et al. (1991)
	Cavada et al. (2000)
	Erickson and Lewis (2004)
	Giguere and Goldman-Rakic (1988)
	Goldman-Rakic and Porrino (1985)
	Hsu and Price (2007)
	Jakab et al. (2012)
	Jang and Yeo (2014)
	Kievit and Kuypers (1977)
	Klein et al. (2010)
	McFarland and Haber (2002)
	Morecraft et al. (1992)
	Ray and Price (1993)
	Romanski et al. (1997)
	Russchen et al. (1987)
	Siwek and Pandya (1991)
	Tobias (1975)
	Xiao et al. (2009)
	Yeterian and Pandya (1988)
	Yeterian and Pandya (1994)
Midline Nuclear Group Paratenial Nucleus Paraventricular Nucleus Reuniens Nucleus	Barbas et al. (1991)
	Cavada et al. (2000)
	Hsu and Price (2007)
	Morecraft et al. (1992)
	Yeterian and Pandya (1988)
Intralaminar Nuclear Group Centromedian Nucleus Parafascicular Nucleus Paracentral Nucleus Central Nuclei	Barbas et al. (1991)
	Cavada et al. (2000)
	Hsu and Price (2007)
	Kievit and Kuypers (1977)
	Morecraft et al. (1992)
	Yeterian and Pandya (1988)
Lateral Nuclear Group Medial Pulvinar Nucleus	Barbas et al. (1991)
	Bos and Benevento (1975)
	Cavada et al. (2000)
	Kievit and Kuypers (1977)
	Morecraft et al. (1992)
	Romanski et al. (1997)
	Trojanowski and Jacobson (1976)

Table 2 (continued)

Thalamic Nuclei	References
Ventral Nuclear Group Ventral Anterior Nucleus Ventral Lateral Nucleus	Barbas et al. (1991)
	Cavada et al. (2000)
	Hsu and Price (2007)
	Kievit and Kuypers (1977)
	Morecraft et al. (1992)
	Yeterian and Pandya (1988)
Posterior Nuclear Group Suprageniculate Nucleus Limitans Nucleus	Barbas et al. (1991)
	Cavada et al. (2000)
	Morecraft et al. (1992)
	Romanski et al. (1997)
Area X	Barbas et al. (1991)
	Cavada et al. (2000)

the VC/VS region. Figure 7 shows the postoperative CT scan registered to the preoperative MRI, demonstrating correct lead placement. Correct placement was also verifiable by the good clinical response described earlier. As shown in Fig. 8, the two sets of fiber connections we reconstructed using two-tensor diffusion tractography, i.e., lOFC-thal (in red) and mOFC-thal (in blue), display an array of virtual fibers as they course from their origins to terminations that resembles a "cloud." Contact 0 of the implant, which is just below the anterior commissure, appears to engage mostly with lateral orbitothalamic fibers, whereas contact 1, which is above the anterior commissure, seems to stimulate also medial orbitothalamic fibers. The tip of the implant, which corresponds to its most distal contact (i.e., contact 0), is clearly shown in direct contact with the center of mass of the lOFC-thal tract in Fig. 8.

Discussion

In the present investigation we mapped the connections of the lateral and the medial orbitofrontothalamic connections and demonstrated their inter-individual anatomical variabillity in the VC/VS region in a sample of 29 individuals using two-tensor diffusion tractography of Connectome data. These observations indicate the potential importance of a tractography-guided, patient-specific approach in DBS surgery for OCD and represent an initial proof of concept in this regard.

Topographic anatomy of the VC/VS region and orbitofrontal circuitries Anatomical knowledge of the VC/VS region, and the ability to delineate the relevant gray matter structures related to its anatomy and to map the fibers of passage within this area, are critical for an accurate target engagement in DBS. In this analysis we elaborated upon the rationale of assessing diffusion

Fig. 4 Variability study in 29 healthy subjects. The center of mass (COM) for each of the 29 subjects is represented as a line in 3-D for both fiber tracts (lOFC-thal, in *red*; mOFC-thal, in *blue*) in panel **a**, whereas in panel **b** the average line of these 29 lines is shown also in 3-D. In panel **c**, the complete distribution of the center of mass of the lOFC-thal (in *red*) and mOFC-thal (in *blue*) fiber tracts in 29 subjects at the anterior commissure (ac) coronal plane of the MNI atlas template, is shown in 2-D, represented as a total of 29 *red* and 29 *blue dots*. In panel **d**, the center of mass across all 29 fiber tracts is represented as a *single dot* at the ac coronal level. R = right; L = left
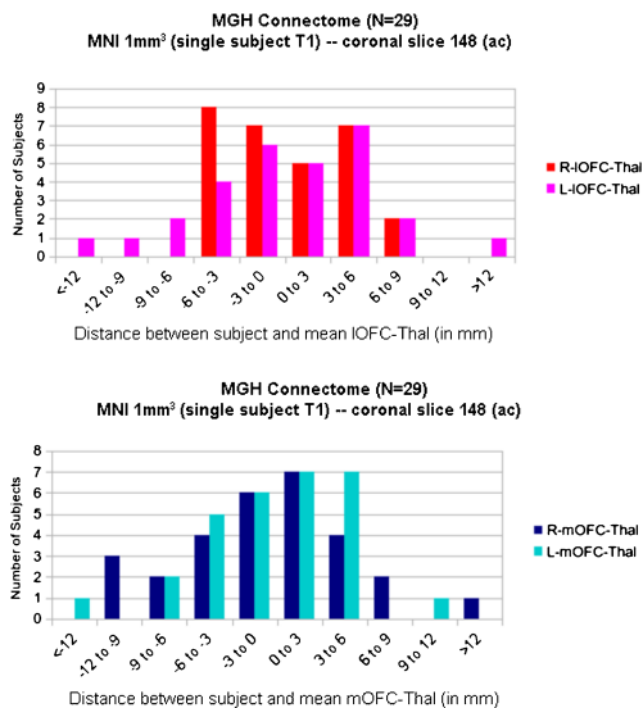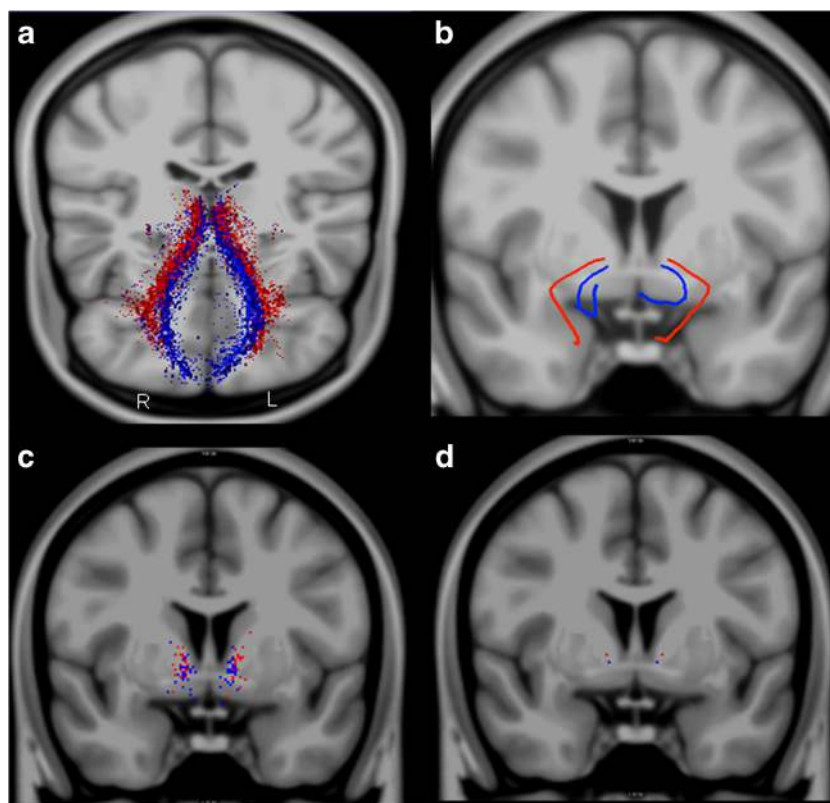

Fig. 5 Histograms showing the distribution of the two fiber tracts connecting the thalamus with the lateral orbitofrontal (lOFC, in *red* and *pink*) and medial orbitofrontal (mOFC, in *light* and *dark blue*) cortex (i.e., lOFC-thal and mOFC-thal, respectively) as a function of distance (in mm) from their overall center at the coronal level of the anterior commissure (ac). *Negative values* denote ventral location, whereas *positive values* indicate dorsal location with respect to the overall center. R = right; L = left

tractography-guided DBS for OCD using the lateral and medial orbitofrontal circuitries as an exemplary paradigm, especially because of the clinical relevance of the lateral orbitofrontothalamic fibers for OCD. The lateral orbitofrontal cortex corresponds to Brodmann's area (BA) 47/12, and its primary circuitry involves reciprocal connections with supracallosal BA 24 and 32, dorsolateral temporal pole (BA 38), inferior temporal cortex (BA 20), the supplementary eye field in the dorsal portion of BA 6, the mediodorsal nucleus of thalamus, dorsal and caudal portions of the basal amygdala and the accessory (magnocellular) basal amygdala (Mega et al. 2005). The circuitry of lOFC is quite different from that of the medial OFC (BA 14), which involves mainly the infracallosal BA 25, 24 and 32, the ventromedial temporal pole (BA 38), the anterior (agranular) insula, the anterior entorhinal cortex (BA 36), the mediodorsal nucleus of thalamus, the medial portion of the basal amygdala, and the accessory basal (magnocellular) amygdala (Mega et al. 2005). Indeed, our results showed connections with several thalamic nuclei, including mediodorsal, anterior medial, midline-intralaminar, and medial pulvinar, in agreement with existing literature in humans and non-human primates (Arikuni et al. 1983; Barbas et al. 1991; Goldman-Rakic and Porrino 1985; Hsu and Price 2007; Jakab et al. 2012; Klein et al. 2010; Morecraft et al. 1992; Ray and Price 1993; Romanski et al. 1997; Yeterian and Pandya 1994;
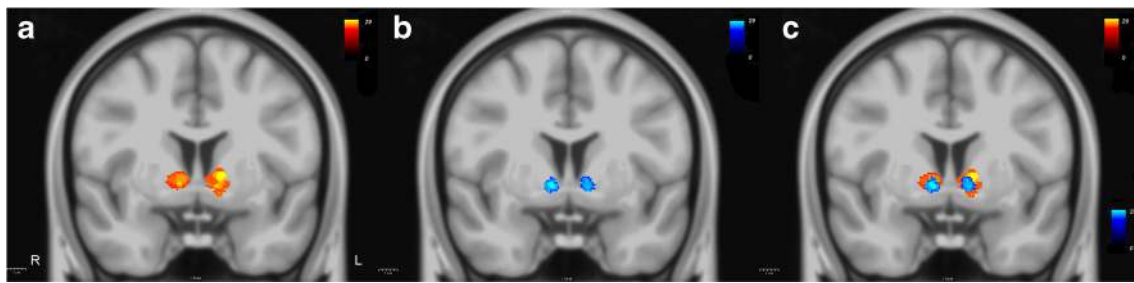
Fig. 6 Heat maps showing the probability distribution of the two fiber tracts connecting the thalamus with the lateral orbitofrontal (lOFC-thal, in yellow and red, in panel **a**) and medial orbitofrontal (mOFC-thal, in *light* and *dark blue*, in panel **b**) cortex in a coronal section at the anterior commissure (ac) level of the MNI atlas template, a standard stereotactic space on which all subjects were previously registered (Evans et al. 1993). Panel **c** shows the relative location of the heat maps of these two fiber tracts. *Color scale bars* represent the range of values (0 to 29 subjects), a measure of the overlap of a certain number of subjects for a given voxel. R = right; L = left

Jang and Yeo 2014). A summary of lOFC-thalamic connectivity is provided in Table 2. In nonhuman primate studies, although several specific lOFC-thalamic connectional relationships have been established, the fine details of the various fiber trajectories have not been determined. The trajectories of fiber pathways between lOFC and specific thalamic nuclei in the human brain remain an open question and are outside the scope of the present investigation.
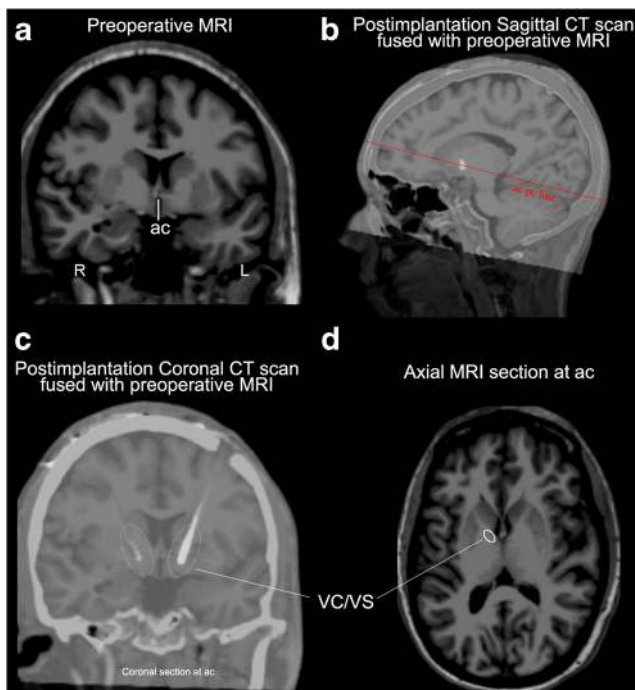

Fig. 7 Preoperative coronal MRI at the anterior commissure (ac) level (**a**) and postimplantation sagittal CT scan fused with preoperative MRI (**b**) showing the position of the implanted electrodes in a patient with OCD who had DBS surgery. In plane (**c**) the co-registration of postimplantation CT scan with the preoperative MRI allows the precise anatomical identification of the implant and its contacts within the ventral capsule/ventral striatum (VC/VS) region. An axial MRI section (**d**) of the same individual at the ac level indicates the location of the VC/VS region in the caudal part of the anterior limb of the internal capsule (ALIC). R = right; L = left; pc = posterior commissure

Inter-subject variability of fibers of passage in the VC/VS region As we have already demonstrated and discussed, within the orbitofrontothalamic circuitry there are distinct populations of fibers subserving different connections and functions. In the context of OCD pathophysiology and clinical features, the orbitofrontothalamic connection is thought to be the most important component within the CSTC circuitry (Fineberg et al. 2010; Graybiel and Rauch 2000). From our preliminary observations, it appears that two-tensor diffusion tractography can accurately trace the fiber connections between OFC and thalamus. These fiber tracts may have different trajectories and positions within the VC/VS area, and precise knowledge of their spatial deployment and relationships may be valuable for the neurosurgeon performing DBS. A small misplacement of the electrode (by a few millimeters) could result in excitation of a markedly different neural circuit in the brain. This may be reflected in terms of therapeutic response (responders vs. non-responders). Future studies could use the techniques described herein to directly assess the correlation between patient response and DBS location relative to key fiber bundles. Another important issue that can be addressed using diffusion tractography is inter-subject variability of the fibers of passage in the VC/VS region. From these preliminary results, we can appreciate the large spatial variability of these fiber tracts of passage in the VC/VS region. Taking this into account could improve the accuracy of DBS electrode placement.

DBS electrode placement and targeting in the VC/VS region in patients with OCD A critical question is which passing fibers are actually engaged by the contacts in the VC/VS region. As shown in Fig. 8, the two fiber connections we reconstructed using two-tensor diffusion tractography, i.e., lOFC-thal (in red) and mOFC-thal (in blue), display an array of virtual fibers that resembles a "cloud" as they course from their origins to terminations. These two clouds run side-by-side but also are intertwined. This morphological anatomical observation may have clinical relevance. Due to the tight and
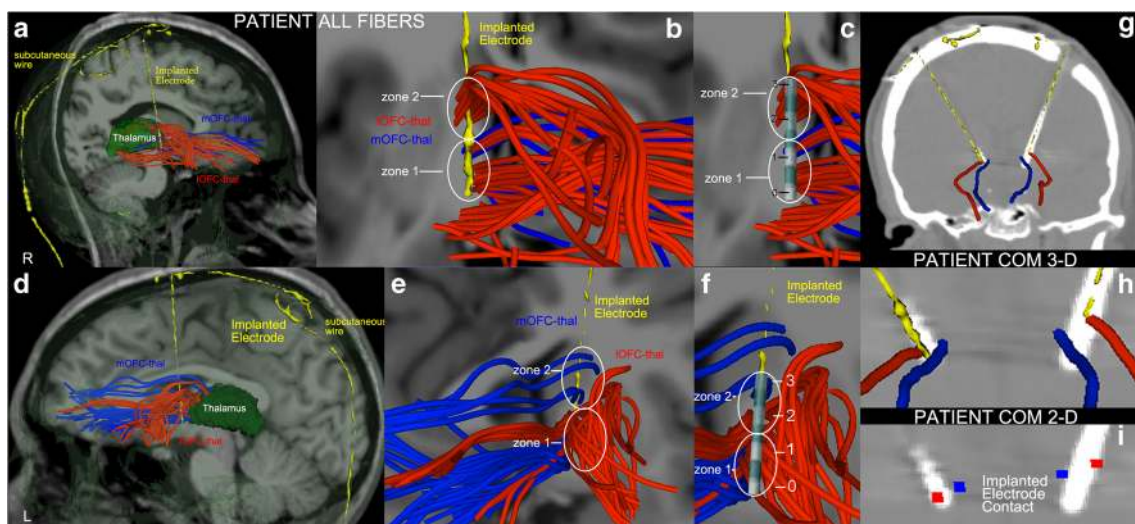
Fig. 8 Fiber tract reconstruction of OFC-thalamic connections using two-tensor diffusion tractography in the *right* (**a**) and *left* (**b**) hemispheres of a patient with OCD who had DBS neurosurgery bilaterally. The two fiber tracts are lOFC-thal (in *red*) and mOFC-thal (in *blue*). Their morphology resembles that of a "cloud" containing intertwined fibers of both tracts running side-by-side in the VC/VS region, which poses the question of how anatomically specific the target engagement by an electrode contact can be. A contact in zone 1 in the left hemisphere (**e**) and in zones 1 and 2 in the right hemisphere (**b**) would stimulate both lOFC-thal (*red*) and mOFC-thal (*blue*) fibers. By contrast, a contact in zone 2 of the left hemisphere (**e**) would stimulate fibers of lOFC-thal (*red*) only. Contacts 0 and 1 in both hemispheres (C-right, F-left) were situated in regions containing both lOFC-thal and mOFC-thal fibers. Contact 2 in both hemispheres (C-right, F-left) and contact 3 in the right hemisphere (**c**) engaged only lOFC-thal fibers, whereas contact 3 in the left hemisphere (**f**) engaged only mOFC-thal fibers. Panels **g**, **h** and **i** show post-implantation CT scans with electrodes and depict the center of mass line (COM line) representation of the lOFC-thal (in *red*) and mOFC-thal (in *blue*) fiber tracts and their spatial relationships with the electrode implant in augmented visualizations in 3-D (panel **h**) and 2-D (I). R = right; L = left; numbers 0, 1, 2 and 3 represent the four contacts of the lead

unpredictable topographic relationships and proximity of these passing fibers, the electrode contact could differentially engage either or both of these connections. Given this fiber arrangement, how anatomically-specific can the target engagement by an electrode contact be? Given the specific circuitries with which the lOFC and mOFC are associated, what are the different behavioral outcomes produced by relatively greater or lesser engagement of each? How may the anatomical specificity of target engagement be associated with therapeutic efficacy ("responders" vs. "non-responders")? Diffusion tractography can define this critical anatomy and thus help determine which fibers of passage are actually stimulated. For instance, a contact in zone 1 in the left hemisphere and in zones 1 and 2 in the right hemisphere would stimulate both lOFC-thal (red) and mOFC-thal (blue). By contrast, a contact in zone 2 of the left hemisphere would stimulate fibers of lOFC-thal (red) only. This case illustrates the complexity of the anatomy in the VC/VS region. It also illustrates the difficulty of determining the anatomical specificity of target engagment in DBS for OCD. Moreover, it emphasizes the necessity of knowing the precise anatomy of the target as a condition for establishing anatomical-clinical correlations to clarify the systems biology underlying clinical outcomes.

We also approached the problem of visualizing fiber tracts in the target zone by reducing the cloud of individual fibers of each tract to a single line, which is their "center of mass" (COM)

representation (Makris et al. 2013a, b). The *COM line representation of a fiber tract* can be shown in 3-D and 2-D and may be useful in a number of ways. First, it provides a quick and clear visualization of the bulk relative topography of the fiber tracts in the target anatomical area (VC/VS in this instance). Second, it enables visualization of several fiber tracts in relatively small areas, where their relative topographies or even the smaller of them may not be visible in the midst of several other larger ones. Third, and importantly, it may provide a metric for targeting and modeling. For example, we could consider a DBS programming algorithm that tried to minimize the Euclidean distance from the core of a given fiber tract to either a contact or a volume of electrical tissue activation. The COM representation may also provide a sound conceptual approach for fiber tract anatomy, given that it simplifies representation of complex trajectories and their topographic relationships. Finally, this approach of visualizing multiple fiber tracts of passage would provide a means to assess inter-subject variability. In the current standard of care in DBS for OCD, the electrodes are implanted stereotaxically in a location that corresponds on average in close proximity to the anterior commissure and with Talairach coordinates that are approximately X (mediolateral dimension) = 6.5 mm, Y (anteroposterior dimension) = 0 mm and Z (dorsoventral dimension) = 3.5 mm (Greenberg et al. 2010a). The patient case illustrated herein showed favorable clinical outcome after 6 months of DBS setting titration following bilateral VC/VS monopolar

implantation. In this case, a 3387 lead was used, which has 1.5 mm contacts with 1.5 mm spacing between them. The contacts 0 and 1 in both hemispheres were situated in regions containing both lOFC-thal and mOFC-thal fibers. Contact 2 in both hemispheres and contact 3 in the right hemisphere engaged only lOFC-thal fibers, whereas contact 3 in the left hemisphere engaged only mOFC-thal fibers (Fig. 8). In this patient, specfically contact 1 was stimulated bilaterally, resulting in both sets of fiber connections being stimulated in the VC/VS region. Thus, the COM representation as well as the more detailed "cloud" representation of fiber tracts provided specific knowledge of target engagement (Fig. 8).

Limitations

There are certain limitations that should be pointed out with respect to the diffusion imaging methodology itself. Diffusion imaging detects and measures water behavior only in extracellular space, making diffusion measures only indirectly related to tract integrity and/or orientation. However, our sample of 29 subjects was relatively large and the diffusion data we acquired were of high quality and resolution. Furthermore, filtered multi-tensor tractography, which significantly improves the angular resolution at crossings and branchings, allows us to trace fibers in regions where multiple axons or tracts cross one another. This results in fewer fiber truncations, more virtual fibers, and more connections. Thus, it seems that multi-tensor tractography is an appropriate technique for the study of inter-individual variability, a topic of great interest in biology. Finally, with respect to the patient case illustrated herein, while the study on variability of the VC/VS tracts is quite reliable, the data used for the patient may affect how well we can construct the VC/VS fibers of passage. However, unless a comparison with Connectome data in patients is done, we are not able to determine this with certainty. It must be pointed out that future, adequately powered studies are needed to determine precisely the optimal parameters for target engagement in OCD DBS treatment as well as the use of metrics such as volume of tissue activated (VTA) for the assessment of the spatial extent of DBS (Chaturvedi et al. 2013).

Conclusions

By mapping and measuring the inter-individual anatomical variability of lOFC-thal and mOFC-thal connections in a sample of 29 individuals using two-tensor diffusion tractography of Connectome data we formulated an initial proof of concept indicating the relevance of a tractography-guided patient-specific approach in DBS neurosurgery for medically intractable OCD. This is in contrast to current surgical practice, which involves implanting all patients at identical stereotactic coordinates within the VC/VS region. We believe that a patient-specific approach

can enhance the efficacy of DBS in the treatment of intractable OCD.

References

Ahmari, S. E., Spellman, T., Douglass, N. L., Kheirbek, M. A., Simpson, H. B., Deisseroth, K., et al. (2013). Repeated cortico-striatal stimulation generates persistent OCD-like behavior. *Science, 340*(6137), 1234–1239. doi:10.1126/science.1234733.

Andrew, J., & Watkins, S. (1969). *A stereotaxic atlas of the human thalamus and adjacent structures; a variability study*. Baltimore: Williams & Wilkins.

Anticevic, A., Hu, S., Zhang, S., Savic, A., Billingslea, E., Wasylink, S., et al. (2014). Global resting-state functional magnetic resonance imaging analysis identifies frontal cortex, striatal, and cerebellar dysconnectivity in obsessive-compulsive disorder. *Biological Psychiatry, 75*(8), 595–605. doi:10.1016/j.biopsych.2013.10.021.

Arikuni, T., Sakai, M., & Kubota, K. (1983). Columnar aggregation of prefrontal and anterior cingulate cortical cells projecting to the thalamic mediodorsal nucleus in the monkey. *Journal of Comparative Neurology, 220*(1), 116–125. doi:10.1002/cne.902200111.

Ayuso-Mateos, J. (2002). *Global burden of obsessive compulsive disorders in the year 2000*. Geneva: World Health Organization.

Barbas, H., Henion, T. H., & Dermon, C. R. (1991). Diverse thalamic projections to the prefrontal cortex in the rhesus monkey. *Journal of Comparative Neurology, 313*(1), 65–94. doi:10.1002/cne.903130106.

Basser, P. J. (2004). Scaling laws for myelinated axons derived from an electrotonic core-conductor model. *Journal of Integrative Neuroscience, 3*(2), 227–244.

Baumgartner, C., Pasternak, O., Bouix, S., Westin, C. F., Rathi, Y. (2012). *Filtered multi-tensor tractography using free water estimation*. Paper presented at the ISMRM, Melbourne, Australia.

Behrens, T. E., Berg, H. J., Jbabdi, S., Rushworth, M. F., & Woolrich, M. W. (2007). Probabilistic diffusion tractography with multiple fibre orientations: What can we gain? *Neuroimage, 34*(1), 144–155, doi:10.1016/j.neuroimage.2006.09.018.

Bonmassar, G., & Makris, N. (2015). *Connectome Pathways in Parkinson's Disease Patients with Deep Brain Stimulators.* Paper presented at the Cogn Int Conf Adv Cogn Technol Appl, Nice, France.

Bos, J., & Benevento, L. A. (1975). Projections of the medial pulvinar to orbital cortex and frontal eye fields in the rhesus monkey (Macaca mulatta). *Experimental Neurology, 49*(2), 487–496.

Burguiere, E., Monteiro, P., Feng, G., & Graybiel, A. M. (2013). Optogenetic stimulation of lateral orbitofronto-striatal pathway suppresses compulsive behaviors. *Science, 340*(6137), 1243–1246. doi:10.1126/science.1232380.

Cavada, C., Company, T., Tejedor, J., Cruz-Rizzolo, R. J., & Reinoso-Suarez, F. (2000). The anatomical connections of the macaque monkey orbitofrontal cortex. A review. *Cerebral Cortex, 10*(3), 220–242.

Chaturvedi, A., Lujan, J. L., & McIntyre, C. C. (2013). Artificial neural network based characterization of the volume of tissue activated during deep brain stimulation. *Journal of Neural Engineering, 10*(5), 056023, doi:10.1088/1741-2560/10/5/056023.

Cuthbert, B. N., & Insel, T. R. (2010). Toward new approaches to psychotic disorders: the NIMH research domain criteria project. *Schizophrenia Bulletin, 36*(6), 1061–1062. doi:10.1093/schbul/sbq108.

Cuthbert, B. N., & Insel, T. R. (2013). Toward the future of psychiatric diagnosis: the seven pillars of RDoC. *BMC Medicine, 11*, 126. doi:10.1186/1741-7015-11-126.

Dale, A. M., Fischl, B., & Sereno, M. I. (1999). Cortical surface-based analysis. I. Segmentation and surface reconstruction. *NeuroImage, 9*(2), 179–194. doi:10.1006/nimg.1998.0395.

Desikan, R. S., Segonne, F., Fischl, B., Quinn, B. T., Dickerson, B. C., Blacker, D., et al. (2006). An automated labeling system for subdividing the human cerebral cortex on MRI scans into gyral based regions of interest. *NeuroImage, 31*(3), 968–980. doi:10.1016/j.neuroimage.2006.01.021.

Dougherty, D. D., Rauch, S. L., Greenberg, B. D. (2010). Pathophysiology of obsessive-compulsive disorders. In D. J. Stein, E. Hollander, R. B. O. (Eds.), *Textbook of Anxiety Disorders* (2nd ed.). Washington, D.C.: APPI; Edinburgh : Compass Academic [distributor].

Erickson, S. L., & Lewis, D. A. (2004). Cortical connections of the lateral mediodorsal thalamus in cynomolgus monkeys. *Journal of Comparative Neurology, 473*(1), 107–127. doi:10.1002/cne.20084.

Evans, A. C., Collins, D. L., Mills, S. R., Brown, E. D., Kelly, R. L., Peters, T. M. (1993). *3D statistical neuroanatomical model from 305 MRI volumes.* Paper presented at the Nuclear Science Symposium and Medical Imaging Conference.

Fineberg, N. A., Potenza, M. N., Chamberlain, S. R., Berlin, H. A., Menzies, L., Bechara, A., et al. (2010). Probing compulsive and impulsive behaviors, from animal models to endophenotypes: a narrative review. *Neuropsychopharmacology, 35*(3), 591–604. doi:10.1038/npp.2009.185.

Fischl, B., & Dale, A. M. (2000). Measuring the thickness of the human cerebral cortex from magnetic resonance images. *Proceedings of the National Academy of Sciences of the United States of America, 97*(20), 11050–11055. doi:10.1073/pnas.200033797.

Fischl, B., Sereno, M. I., & Dale, A. M. (1999). Cortical surface-based analysis. II: inflation, flattening, and a surface-based coordinate system. *NeuroImage, 9*(2), 195–207. doi:10.1006/nimg.1998.0396.

Fischl, B., Salat, D. H., Busa, E., Albert, M., Dieterich, M., Haselgrove, C., et al. (2002). Whole brain segmentation: automated labeling of neuroanatomical structures in the human brain. *Neuron, 33*(3), 341–355.

Fischl, B., van der Kouwe, A., Destrieux, C., Halgren, E., Segonne, F., Salat, D. H., et al. (2004). Automatically parcellating the human cerebral cortex. *Cerebral Cortex, 14*(1), 11–22.

Galaburda, A. M., Corsiglia, J., Rosen, G. D., & Sherman, G. F. (1987). Planum temporale asymmetry, reappraisal since Geschwind and Levitsky. *Neuropsychologia, 25*(6), 853–868.

Giguere, M., & Goldman-Rakic, P. S. (1988). Mediodorsal nucleus: areal, laminar, and tangential distribution of afferents and efferents in the frontal lobe of rhesus monkeys. *Journal of Comparative Neurology, 277*(2), 195–213. doi:10.1002/cne.902770204.

Goldman-Rakic, P. S., & Porrino, L. J. (1985). The primate mediodorsal (MD) nucleus and its projection to the frontal lobe. *Journal of Comparative Neurology, 242*(4), 535–560. doi:10.1002/cne.902420406.

Graybiel, A. M., & Rauch, S. L. (2000). Toward a neurobiology of obsessive-compulsive disorder. *Neuron, 28*(2), 343–347.

Greenberg, B. D., Gabriels, L. A., Malone, D. A., Jr., Rezai, A. R., Friehs, G. M., Okun, M. S., et al. (2010a). Deep brain stimulation of the ventral internal capsule/ventral striatum for obsessive-compulsive disorder: worldwide experience. *Molecular Psychiatry, 15*(1), 64–79. doi:10.1038/mp.2008.55.

Greenberg, B. D., Rauch, S. L., & Haber, S. N. (2010b). Invasive circuitry-based neurotherapeutics: stereotactic ablation and deep brain stimulation for OCD. *Neuropsychopharmacology, 35*(1), 317–336. doi:10.1038/npp.2009.128.

Greist, J. H., Jefferson, J. W., Kobak, K. A., Katzelnick, D. J., & Serlin, R. C. (1995). Efficacy and tolerability of serotonin transport inhibitors in obsessive-compulsive disorder. A meta-analysis. *Archives of General Psychiatry, 52*(1), 53–60.

Hsu, D. T., & Price, J. L. (2007). Midline and intralaminar thalamic connections with the orbital and medial prefrontal networks in macaque monkeys. *Journal of Comparative Neurology, 504*(2), 89–111. doi:10.1002/cne.21440.

Jakab, A., Blanc, R., & Berenyi, E. L. (2012). Mapping changes of in vivo connectivity patterns in the human mediodorsal thalamus: correlations with higher cognitive and executive functions. *Brain Imaging and Behavior, 6*(3), 472–483. doi:10.1007/s11682-012-9172-5.

Jang, S. H., & Yeo, S. S. (2014). Thalamocortical connections between the mediodorsal nucleus of the thalamus and prefrontal cortex in the human brain: a diffusion tensor tractographic study. *Yonsei Medical Journal, 55*(3), 709–714. doi:10.3349/ymj.2014.55.3.709.

Jbabdi, S., Lehman, J. F., Haber, S. N., & Behrens, T. E. (2013). Human and monkey ventral prefrontal fibers use the same organizational principles to reach their targets: tracing versus tractography. *Journal of Neuroscience, 33*(7), 3190–3201. doi:10.1523/JNEUROSCI.2457-12.2013.

Kievit, J., & Kuypers, H. G. (1977). Organization of the thalamo-cortical connexions to the frontal lobe in the rhesus monkey. *Experimental Brain Research, 29*(3–4), 299–322.

Klein, J. C., Rushworth, M. F., Behrens, T. E., Mackay, C. E., de Crespigny, A. J., D'Arceuil, H., et al. (2010). Topography of connections between human prefrontal cortex and mediodorsal thalamus studied with diffusion tractography. *NeuroImage, 51*(2), 555–564. doi:10.1016/j.neuroimage.2010.02.062.

Koran, L. M., Hanna, G. L., Hollander, E., Nestadt, G., Simpson, H. B., & American Psychiatric, A. (2007). Practice guideline for the treatment of patients with obsessive-compulsive disorder. *The American Journal of Psychiatry, 164*(7 Suppl), 5–53.

Laidlaw, T. M., Falloon, I. R., Barnfather, D., & Coverdale, J. H. (1999). The stress of caring for people with obsessive compulsive disorders. *Community Mental Health Journal, 35*(5), 443–450.

Lehman, J. F., Greenberg, B. D., McIntyre, C. C., Rasmussen, S. A., & Haber, S. N. (2011). Rules ventral prefrontal cortical axons use to reach their targets: implications for diffusion tensor imaging tractography and deep brain stimulation for psychiatric illness.

Journal of Neuroscience, 31(28), 10392–10402. doi:10.1523/JNEUROSCI.0595-11.2011.

Makris, N., Meyer, J. W., Bates, J. F., Yeterian, E. H., Kennedy, D. N., & Caviness, V. S. (1999). MRI-Based topographic parcellation of human cerebral white matter and nuclei II. Rationale and applications with systematics of cerebral connectivity. *NeuroImage, 9*(1), 18–45. doi:10.1006/nimg.1998.0384.

Makris, N., Preti, M. G., Asami, T., Pelavin, P., Campbell, B., Papadimitriou, G. M., et al. (2013a). Human middle longitudinal fascicle: variations in patterns of anatomical connections. *Brain Structure and Function, 218*(4), 951–968. doi:10.1007/s00429-012-0441-2.

Makris, N., Preti, M. G., Wassermann, D., Rathi, Y., Papadimitriou, G. M., Yergatian, C., et al. (2013b). Human middle longitudinal fascicle: segregation and behavioral-clinical implications of two distinct fiber connections linking temporal pole and superior temporal gyrus with the angular gyrus or superior parietal lobule using multi-tensor tractography. *Brain Imaging and Behavior, 7*(3), 335–352. doi:10.1007/s11682-013-9235-2.

Malcolm, J. G., Shenton, M. E., & Rathi, Y. (2010). Filtered multitensor tractography. *IEEE Transactions on Medical Imaging, 29*(9), 1664–1675. doi:10.1109/TMI.2010.2048121.

Mancebo, M. C., Greenberg, B., Grant, J. E., Pinto, A., Eisen, J. L., Dyck, I., et al. (2008). Correlates of occupational disability in a clinical sample of obsessive-compulsive disorder. *Comprehensive Psychiatry, 49*(1), 43–50. doi:10.1016/j.comppsych.2007.05.016.

McFarland, N. R., & Haber, S. N. (2002). Thalamic relay nuclei of the basal ganglia form both reciprocal and nonreciprocal cortical connections, linking multiple frontal cortical areas. *Journal of Neuroscience, 22*(18), 8117–8132.

Mega, M. S., Cummings, J. L., Salloway, S., Malloy, P. (2005). The limbic system. In *The neuropsychiatry of limbic and subcortical disorders* (pp. 3–18): American Psychiatric Press, Inc.

Milad, M. R., & Rauch, S. L. (2012). Obsessive-compulsive disorder: beyond segregated cortico-striatal pathways. *Trends in Cognitive Sciences, 16*(1), 43–51. doi:10.1016/j.tics.2011.11.003.

Morecraft, R. J., Geula, C., & Mesulam, M. M. (1992). Cytoarchitecture and neural afferents of orbitofrontal cortex in the brain of the monkey. *Journal of Comparative Neurology, 323*(3), 341–358. doi:10.1002/cne.903230304.

Pallanti, S., Hollander, E., Bienstock, C., Koran, L., Leckman, J., Marazziti, D., et al. (2002). Treatment non-response in OCD: methodological issues and operational definitions. *International Journal of Neuropsychopharmacology, 5*(2), 181–191. doi:10.1017/S1461145702002900.

Pauls, D. L., Abramovitch, A., Rauch, S. L., & Geller, D. A. (2014). Obsessive-compulsive disorder: an integrative genetic and neurobiological perspective. *Nature Reviews Neuroscience, 15*(6), 410–424. doi:10.1038/nrn3746.

Pittenger, C., & Bloch, M. H. (2014). Pharmacological treatment of obsessive-compulsive disorder. *The Psychiatric Clinics of North America, 37*(3), 375–391. doi:10.1016/j.psc.2014.05.006.

Posner, J., Marsh, R., Maia, T. V., Peterson, B. S., Gruber, A., & Simpson, H. B. (2014). Reduced functional connectivity within the limbic cortico-striato-thalamo-cortical loop in unmedicated adults with obsessive-compulsive disorder. *Human Brain Mapping, 35*(6), 2852–2860. doi:10.1002/hbm.22371.

Rathi, Y., Gagoski, B., Setsompop, K., Michailovich, O., Grant, P. E., & Westin, C. F. (2013). Diffusion propagator estimation from sparse measurements in a tractography framework. *Med Image Comput Comput Assist Interv, 16*(Pt 3), 510–517.

Rathi, Y., Malcolm, J. G., Bouix, S., Westin, C. F., & Shenton, M. (2010). *False positive detection using filtered tractography.* Paper presented at the International Society For Magnetic Resonance in Medicine Scientific Meeting (ISMRM), Stockholm.

Ray, J. P., & Price, J. L. (1993). The organization of projections from the mediodorsal nucleus of the thalamus to orbital and medial prefrontal cortex in macaque monkeys. *Journal of Comparative Neurology, 337*(1), 1–31. doi:10.1002/cne.903370102.

Romanski, L. M., Giguere, M., Bates, J. F., & Goldman-Rakic, P. S. (1997). Topographic organization of medial pulvinar connections with the prefrontal cortex in the rhesus monkey. *Journal of Comparative Neurology, 379*(3), 313–332.

Russchen, F. T., Amaral, D. G., & Price, J. L. (1987). The afferent input to the magnocellular division of the mediodorsal thalamic nucleus in the monkey, Macaca fascicularis. *Journal of Comparative Neurology, 256*(2), 175–210. doi:10.1002/cne.902560202.

Setsompop, K., Kimmlingen, R., Eberlein, E., Witzel, T., Cohen-Adad, J., McNab, J. A., et al. (2013). Pushing the limits of in vivo diffusion MRI for the human connectome project. *NeuroImage, 80*, 220–233. doi:10.1016/j.neuroimage.2013.05.078.

Siwek, D. F., & Pandya, D. N. (1991). Prefrontal projections to the mediodorsal nucleus of the thalamus in the rhesus monkey. *Journal of Comparative Neurology, 312*(4), 509–524. doi:10.1002/cne.903120403.

Song, S. K., Sun, S. W., Ramsbottom, M. J., Chang, C., Russell, J., & Cross, A. H. (2002). Dysmyelination revealed through MRI as increased radial (but unchanged axial) diffusion of water. *NeuroImage, 17*(3), 1429–1436.

Song, S. K., Sun, S. W., Ju, W. K., Lin, S. J., Cross, A. H., & Neufeld, A. H. (2003). Diffusion tensor imaging detects and differentiates axon and myelin degeneration in mouse optic nerve after retinal ischemia. *NeuroImage, 20*(3), 1714–1722.

Talairach, J., David, M., Tournoux, P., Corredor, H., & Kvasina, T. (1957). *Atlas d'anatomie stéréotaxique des noyaux gris centraux*. Paris: Masson.

Tobias, T. J. (1975). Afferents to prefrontal cortex from the thalamic mediodorsal nucleus in the rhesus monkey. *Brain Research, 83*(2), 191–212.

Trojanowski, J. Q., & Jacobson, S. (1976). Areal and laminar distribution of some pulvinar cortical efferents in rhesus monkey. *Journal of Comparative Neurology, 169*(3), 371–392. doi:10.1002/cne.901690307.

Wassermann, D., Makris, N., Rathi, Y., Shenton, M., Kikinis, R., Kubicki, M., et al. (2013). On describing human white matter anatomy: the white matter query language. *Med Image Comput Comput Assist Interv, 16*(Pt 1), 647–654.

Xiao, D., & Barbas, H. (2002). Pathways for emotions and memory. II. Afferent input to the anterior thalamic nuclei from prefrontal, temporal, hypotha- lamic areas and the basal ganglia in the rhesus monkey. *Thalamus Related Systems, 2*(1), 33–48.

Xiao, D., Zikopoulos, B., & Barbas, H. (2009). Laminar and modular organization of prefrontal projections to multiple thalamic nuclei. *Neuroscience, 161*(4), 1067–1081. doi:10.1016/j.neuroscience.2009.04.034.

Yang, J. C., Ginat, D. T., Dougherty, D. D., Makris, N., & Eskandar, E. N. (2014). Lesion analysis for cingulotomy and limbic leucotomy: comparison and correlation with clinical outcomes. *Journal of Neurosurgery, 120*(1), 152–163. doi:10.3171/2013.9.JNS13839.

Yang, J. C., Papadimitriou, G., Eckbo, R., Yeterian, E., Liang, L., Dougherty, D. D., et al. (2015). Multi-tensor investigation of orbitofrontal cortex tracts affected in subcaudate tractotomy. *Brain Imaging and Behavior, 9*(2), 342–352. doi:10.1007/s11682-014-9314-z.

Yeterian, E. H., & Pandya, D. N. (1988). Corticothalamic connections of paralimbic regions in the rhesus monkey. *Journal of Comparative Neurology, 269*(1), 130–146. doi:10.1002/cne.902690111.

Yeterian, E. H., & Pandya, D. N. (1994). Laminar origin of striatal and thalamic projections of the prefrontal cortex in rhesus monkeys. *Experimental Brain Research, 99*(3), 383–398.